JOURNAL OF GEOPHYSICAL RESEARCH, VOL. 98, NO. D10, PAGES 18,575–18,587, OCTOBER 20, 1993

One Year of Cloud Lidar Data From Dumont d'Urville (Antarctica) 1. General Overview of Geometrical and Optical Properties

MASSIMO DEL GUASTA, MARCO MORANDI, AND LEOPOLDO STEFANUTTI

Istituto Ricerca Onde Elettromagnetiche of CNR (Florence, Italy)

JACQUES BRECHET AND JACQUES PIQUAD

Expeditions polaires francaises, (Paris, France)

Tropospheric clouds play a major role in climate regulation but, so far, only a few long-term ground-based observations, devoted to the study of the cloud optical and radiative properties, have been carried out. In this work the statistics of 1 year of coastal Antarctic cloud lidar measurements (532 nm) are shown. Cloud macrophysical and optical parameters have been retrieved from lidar returns; radiosonde data allowed us to build statistics of such quantities in terms of cloud temperature. Information about the physical phase of water and ice crystal habit has been obtained from the depolarization and extinction/backscattering ratio; a change in crystal habit (and/or size) around -30 °C is evidenced by the depolarization versus temperature behavior. The extinction/backscattering ratio shows a negative trend with temperature, reflecting microphysical changes. Visible extinction shows wide data dispersion, but with a marked negative trend with temperature. The relative derivatives of extinction and optical depth with temperature have been computed, such quantities result quite constant with temperature.

1. INTRODUCTION

The difficulty in the realistic modelling of the Earth's climate is intrinsically related to the complexity of the studied system. The interactions connecting the "simple" components of atmosphere, ocean, crust and biosphere are little known, even from a qualitative point of view. For this reason, improvement of global circulation models (GCMs) needs a large amount of statistically valid empirical data to be used as a basic input. As a primary rough output, the sensitivity of GCMs to particular phenomena is assessed in order to address further research on the most important links of the chain. Clouds are one such topic, as their effect on the Earth's radiation budget is one of the main uncertainties of GCM outputs [*Cess et al.*, 1990; *Slingo*, 1990]. Actual cloud effect on radiation budget, as observed by satellite, shows strong seasonal and regional variations [*Stephens and Greenwald*, 1991] contributing to a mean surface cooling of about 18°C when compared to a cloudless Earth. Changes in microphysical or macrophysical cloud properties could modify this balance. GCMs predict a vertical and latitudinal change in water vapor distribution as a result of greenhouse gas increase [*Mitchell et al.*, 1989] (as confirmed by satellite data [*Rind et al.*, 1991]). Such models predict a change in cloud frequency, height and composition following greenhouse forcing.

Ground-based lidars working on a routine basis could give useful information for GCM cloud parameterization. A network of such instruments can follow possible changes of macrophysical properties of clouds, giving helpful information about their microphysics. Comparison between lidar and satellite cloud data can largely improve cloud algorithms for satellite data processing. In this spirit, part of the data set presented in this work has been collected in the frame of the *Experimental Cloud Lidar Pilot Study (ECLIPS)* [1988]. Data refer to the Antarctica, a region insufficiently researched in tropospheric studies.

A depolarization backscattering lidar was operated in 1989 and 1990 at the base of Dumont d'Urville (DDU), located on an island a few kilometres off the coast of Antarctica (66° S, 140° E). Cloud data were collected, on a routine basis, 24 h/d. The laser was operated with a 1 pulse/min repetition rate and 10-min averaged profiles were acquired. During the ECLIPS campaigns the laser was operated with a 6-pulse/min repetition rate, while signatures averaged over 1 min were acquired.

Daily balloon soundings and three hourly ground-based meteorological observations are available. Continuous video recording of clouds, LW, and SW radiometric data (wideband - wide-angle PIR and PSP radiometers) and meteorological maps are also available.

2. METHOD FOR INVERTING LIDAR DATA WITH RESPECT TO THE OPTICAL PARAMETERS.

The main characteristics of the lidar system [*Sacco et al.*, 1989] are as follows: A frequency doubled Nd:YAG laser is used as a transmitter. The pulse energy is about 400 mJ at 532 nm with a 10 pps maximun repetition rate and the divergency is about 0.5 mrad (full angle). The receiver is a 0.5-m diameter telescope with a 0.6-mrad (full angle) field of view. A narrowband filter (0.15 nm) and two crossed polarization detection channels are used. The acquisition system (LeCroy) is based on two 8-bit, 32-MHz waveform recorders.

To reduce the global amount of processed data, the optical, geometrical, and meteorological information has been retrieved from lidar profiles averaged over a 30-min standard period. All clear sky profiles have been rejected. A total of 2770 archived data was obtained. Each archived data is represented by a point in a hyperspace whose coordinates are 80 quantities of possible interest computed for each cloud data.

Cloud base, cloud top, midcloud, and the depolarization peak heights are deduced directly from lidar profiles. For all such levels and for each cloud point the temperature,

Paper number 93JD01476.
0148-0227/93/93JD-01476$05.00

temperature lapse rate, pressure, relative humidity, and wind velocity have been computed from the daily meteosonde profiles. Temperature data were obtained as a weighted average of the two closest soundings and have been associated with lidar data only when the nearest sounding occurred within 12 hours around the lidar acquisition time; the horizontal advection (°C/h) has been computed in the layer edged by cloud base and top. Wind data and advection were used only if the closest sounding occurred within 6 hours.

Lidar Equation

We recall that the lidar equation, neglecting the absorption, yields

$$P(z) = E_0 \frac{\tau c}{2} K_L A \frac{\beta(z)}{z^2} \exp[-2\alpha \int_0^z \sigma(z')\, dz]$$

where P(z) is the received power from the range z, Eo is the transmitted pulse energy, c is the light's speed, α is a multiple-scattering factor (averaged through the cloud), A is the receiver effective area, and K_L is a calibration constant; $\beta(z)=\beta_R(z)+\beta_A(z)$ and $\sigma(z)=\sigma_R(z)+\sigma_A(z)$ are the volume backscattering and extinction coefficients. The subscripts R and A indicate the molecular (Rayleigh) and aerosol contribution. Absorption is negligible at 532-nm wavelength. Other definitions used in this work are as follows:

Lidar optical depth δ between cloud base and top

$$\delta = \alpha \int \sigma_A(z)\, dz \quad (1)$$

Scattering ratio R(z)

$$R(z) = \frac{\beta_A(z)+\beta_R(z)}{\beta_R(z)} \quad (2)$$

Mean lidar extinction/backscattering ratio k

$$k = \alpha k' \quad (3)$$

with $0.5 < \alpha < 1$ and

$$k' = \frac{\int \sigma_A(z)dz}{\int \beta_A(z)dz}$$

where k' = k in single scattering; the integration limits are cloud base and top heights.
Two different definitions of depolarization have been used.

$$Dep1(z) = \beta s(z)/\beta p(z) \quad (4)$$

$$Dep2(z) = \beta s_A(z)/\beta p_A(z) \quad (5)$$

Dep1 is computed as the ratio of the "p" and "s" lidar signals, including the molecular contribution, whereas Dep2 computing has been performed taking away the molecular profile from both "p" and "s" lidar returns. The meaning of "p" and "s" is, respectively, parallel and perpendicular with respect to the transmitted beam polarization plane. The conversion between the two depolarizations is given by

$$Dep2 = \frac{a}{(1 - a)} \quad (6)$$

where

$$a = Dep1 \frac{[1 + (R - 1)(D_R + 1)] - D_R}{(D_R + 1)(Dep1 + 1)(R - 1)}$$

The depolarization induced by molecular scattering D_R is given by

$$D_R = \frac{\beta s_R}{\beta p_R} \quad (7)$$

Molecular Density Profiles

Lidar data processing requires reliable molecular density profiles of the atmosphere. For this purpose the daily PTU radiosonde data have been used. Monthly averaged profiles have been produced to evaluate the magnitude of natural fluctuations. Such mean profiles have been also used for lidar data processing when soundings were not available. A polynomial exponential function has been used to fit the density profiles obtained from PTU data

$$d(z) = \exp(c_1 + c_2 z + c_3 z^2 + c_4 z^3 + c_5 z^4) \quad (8)$$

In Figure 1 a fitting of a monthly mean density profile is shown. The coefficients of the polynomial exponent are reported in table 1 for each month in 1989, together with the standard estimation errors. These coefficients are valid between 1 and 15 km.

Lidar Data Inversion

Several inversion methods have been tested [*Klett*, 1981, 1985, *Fernald*, 1984], including a simple iterative

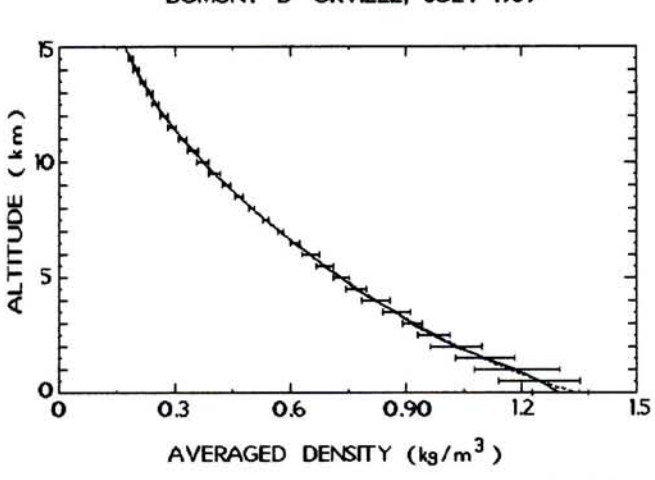

Fig. 1. Monthly averaged air density profile obtained from soundings. One standard deviation bars of natural fluctuations and fitting function described in text (dotted) are shown.

Tab. 1. Polynomial Coefficients of the Air Density Fitting Function

Month	C_1	C_2	C_3	C_4	C_5	See
January	0.255	-1.29E-4	8.57E-9	-1.21E-12	4.21E-17	6E-3
February	0.261	-1.41E-4	1.02E-8	-1.21E-12	3.80E-17	4E-3
March	0.251	-1.15E-4	4.10E-9	-8.36E-13	3.22E-17	5E-3
April	0.274	-1.25E-4	5.28E-9	-8.25E-13	2.89E-17	7E-3
May	0.258	-1.35E-4	8.68E-9	-1.20E-12	4.12E-17	4E-3
June	0.342	-1.73E-4	1.57E-8	-1.70E-12	5.29E-17	2E-3
July	0.294	-1.43E-4	9.12E-9	-1.11E-12	3.55E-17	4E-3
August	0.362	-1.87E-4	1.78E-8	-1.68E-12	4.68E-17	6E-3
September	0.299	-1.47E-4	9.09E-9	-9.08E-13	2.35E-17	2E-3
October	0.315	-1.58E-4	1.14E-8	-1.08E-12	2.75E-17	3E-3
November	0.268	-1.28E-4	7.01E-9	-1.01E-12	3.36E-17	1E-3
December	0.311	-1.71E-4	1.63E-8	-1.72E-12	5.28E-17	4E-3

Read -1.29E-4 as -1.29×10^{-4}. See text, equation (8) for the monthly means of 1989 soundings. Fitting is between 1 and 15 km. Standard estimation error (See) is reported.

numerical solution developed by *Istituto Ricerca Onde Elettromagnetiche (IROE)* group [*Morandi*, 1992]. A simulation program was written to evaluate the errors arising from the inversion of our lidar data and to compare the results obtained by using the different procedures. Tests show that the error magnitude does not depend on the method used for DDU data processing. This is also true in spite of substantial differences between methods, such as different laws that account for the dependence between extinction and backscattering. The program used for cloud lidar profile processing [*Morandi*, 1992] is based on a modified backward *Klett* [1981] routine. The following fundamental steps of the inversion procedure are given:

1.) The cloud base, top, and peak heights are automatically computed from the derivative of the raw signal. Sometimes the automatic method failed and the computed values were corrected by the operator.

2.) The meteosonde data file closest to the lidar acquisition is automatically searched. The five coefficients of the density fitting function (equation (8)) are computed.

3.) The depolarization profile is computed on the basis of the raw "p" and "s" signals.

4.) Both the squared range and the depolarization ratio corrections of the "p" component of the signal are performed.

5.) The lidar return is converted into a backscattering profile by fitting the signal to the molecular density model. The fitting region is chosen below the cloud base in a range where the signal behavior denotes an almost aerosol-free atmosphere.

6.) In the *Klett*'s [1981] solution the law that accounts for the dependence between extinction $\alpha(z)$ and backscattering $\beta(z)$ is assumed the following form:

$$\beta(z) = K1\ \sigma(z)^{k2} \qquad (9)$$

$\beta(z)$ and $\sigma(z)$ include both aerosol and molecular scattering, so that k2 is not equal to 1 (as expected for homogeneous aerosol layers or air separately). Further causes of variability in k2 are found in multiple scattering and in the change of aerosol size distribution within the cloud. The extinction profile $\sigma(z)$ is computed by means of a backward integration of the lidar equation, starting from a reference range z_m and considering a multiple scattering factor $\alpha = 1$ (single scattering). Two different approaches have been used in our analysis

Optically thin cloud (full lidar penetration). The *Klett*'s [1981] method involving only a bound ($\sigma(z_m)$) is not capable of giving a value for k2. If k2 is unknown but assumed constant within the cloud, a second bound below cloud base is necessary. In this study we impose a scattering ratio R = 1 at the cloud base, while the molecular extinction $\sigma_R(z_m)$ is used as a reference value $\sigma(z_m)$. The inversion routine is iterated varying the value of k2 until a good fitting is obtained between the molecular atmosphere profile and the extinction-corrected lidar return, both above and below the cloud.

Optically thick clouds (full lidar extinction). For such cases a scattering ratio R = 1 is assumed at the cloud base. The k2 = 1 is used, while $\sigma(z_m)$ is computed as suggested by *Klett* [1981].

7.) As a final step the lidar return is corrected for the extinction, and the integrated backscattering, optical depth, k parameter, and scattering ratio profile are computed.

Errors due to the inversion. The data set presented in this work has been processed by the same operator in order to reject, with homogeneous criteria, all the data files that are considered too noisy and those showing signs of ambiguous behavior. The primary causes of error in DDU data inversion resulted in the atmospheric density profile approximation and in the arbitrary assumption of R = 1 at cloud base and top.

The ratio between the scattering ratio imposed value (R = 1) and the actual one yields a scaling of the backscattering profile and errors in the extinction computation, while differences in the values of R at the cloud base and top heights introduce errors in the retrieved optical depth. Clear sky lidar profiles have been used to estimate the magnitude of the fluctuation of R with the height within a cloud-free atmosphere. Tests show a good overlapping between lidar-measured and radiosonde-computed molecular profiles with deviations of the order of a few percent. Fluctuation in the scattering ratio of the order of 10% between the cloud base and the top seems to be a reasonable limit value for most of the cases. As a consequence an error of the order of 0.05 should be expected in the retrieved optical depth. The relative error magnitude is a function of the optical depth; the optical depth of subvisual cloud is the most uncertain, with relative errors of 100% and more.

In optically thick clouds, multiple scattering is a further, difficult to assess, source of error. Tests concerning the impact of multiple scattering on extinction and k ratio in DDU cloud are shown in sections 5 and 6. In our work a multiple scattering factor $\alpha = 1$ has been used, taking into account the narrow field of view of the telescope. Due to this assumption, in water clouds with optical depth $> \approx 2$, the retrieved values of the extinction, optical depth, and k are underestimated by about $20 \div 30\%$.

Errors on depolarization profiles. Computing the depolarization ratio requires a calibration of the system; a relative error of about 5% is introduced by calibration and by the receiving optics. Considering processing errors, an estimation of the overall relative accuracy of about 20% seems to be reasonable when neglecting the multiple scattering effect. Multiple scattering affects the depolarization of optically thick clouds, causing an almost linear increase of the depolarization with cloud penetration. The value of such depolarization may reach the order of $10 \div 20\%$ at the top of thicker DDU low clouds. This means that the peak depolarization of such clouds is overestimated. High clouds generally show very uniform depolarization profiles, suggesting that the multiple scattering effect is negligible.

Errors on the optical parameters due to lidar data averaging. In this study each cloud represents a 30-min average. This way, because of cloud variability,

additional errors in the optical parameters are induced. Tests have been performed by processing 60-min-averaged signatures of cloud profiles that showed a strong temporal variability. Results have been compared with those obtained as the average of the values retrieved from 5-min partial averages. Maximum relative differences are +4% for k, ±15% for the integrated backscattering, -13% for the mean backscattering, ±10% for optical depth, and -15% for the mean extinction.

An underestimation of averaged extinction and backscattering of about 10÷20% is expected. The expected relative error on the depolarization peak values is less than -10%.

3. DISCUSSION OF GENERAL METEOROLOGICAL DATA FROM DUMONT D'URVILLE (DDU), 1989.

Meteorological data have been mainly processed together with the corresponding lidar measurements, but a study of the meteorological features of 1989 in DDU has been performed to support cloud data interpretation. Yearly plots of several meteoparameters and monthly averages of radionsonde profiles have been produced.

An inversion layer at 1000÷3000 m was present most of the months. This explains the frequent occurrence of stratified low clouds, as shown in Figure 2, where the cloud top temperature lapse rate is plotted. Most clouds at about -20°C midcloud temperature (about 2000-m height) showed a subadiabatic lapse rate at their top. The warm layer creating the inversion is explained with the subduction of polar air in the lower-tropospheric polar high-pressure centre [*Schwerdtfeger*, 1984]. The 1989 tropopause was 8000-9000 m high, rising up to 10,000 m during the winter. Figure 2 shows that many cirrus clouds reached the tropopause height. During the winter the tropopause often disappeared, and above 13 km the temperature fell down to -75°C (July-September). Higher temperatures in the lower stratosphere and higher troposphere came back at the end of September when DDU was definitively outside the polar stratospheric vortex.

The relative humidity with respect to water was always high (50-75%) up to 5000-6000 meters (at such heights temperature falls below -40°C and the type of sondes used gives unreliable data). Winds coming from northern quadrants (from the sea) bring a higher relative humidity than from southern quadrants, typically 60÷80% against 40÷60%.

According to the zonal circulation of tropospheric polar air, prevailing winds in DDU are westerlies above 3000 m. At lower altitudes, winds are dominated by polar easterlies due to the anticyclonic circulation centred in East Antarctica and the offshore presence of a belt of low-pressure centers [Carleton ,1981]. In the first 1000-m layers, the Ekman rotation of wind direction, breeze, and catabatic wind frictional forcing gives resultant winds with a component from the south and a mean direction of 150° near the ground.

Horizontal advection, computed from daily wind profiles, allows us to identify the different incoming air masses. Negative advection indicates cold continental air, while the arrival of marine air is characterized by positive advection values. Possible differences can be searched for in the optical properties of clouds of the same type but formed under different conditions in air containing different cloud condensation nuclei and water concentrations. As a preliminary result no correlations have been noticed between the optical properties of DDU clouds and the advection sign above 2-3 km (where the hypothesis of geostrophic wind made in advection definition is satisfied).

4. STATISTIC OF CLOUD GEOMETRICAL CHARACTERISTICS

Only during brief time periods could strong snowdrift or snowfall inhibit lidar data acquisition. Few pauses were needed for system maintenance. The following statistics of 1989 clouds is therefore almost complete.

Lidar data are not reliable for clouds with a base lower than 500 m because of the lidar overlap function; cloud top and midcloud have been represented only when reliable and have not been reported for clouds only partially penetrated by the laser. In the presence of multiple layers separated by clean air, a cloud data point has been produced for each layer. Midcloud is obtained from the backscattering profile by using equation (9).

Figures 3, 4, and 5 show the distributions of several geometrical parameters. It is evident that low and midlevel clouds dominated the 1989 lidar data. Two peaks in the

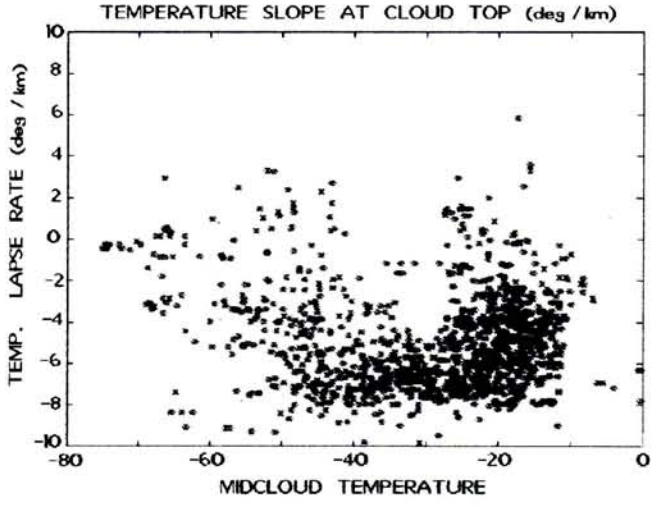

Fig. 2. Temperature lapse rate (dT/dz) in Dumont D'Urville cloud tops, 1989; subadiabatic conditions often occur both in low and high clouds.

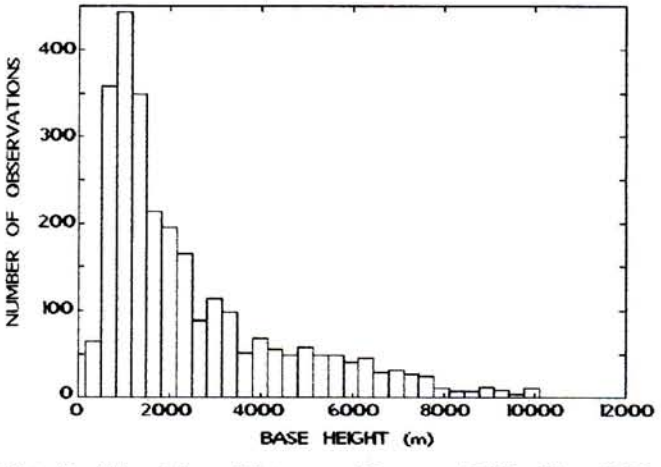

Fig. 3. Cloud base histogram Dumont D'Urville, 1989. The plot is not reliable below 500 m, because very low clouds were out of lidar range. Cloud base is obtained from the derivative of lidar profile.

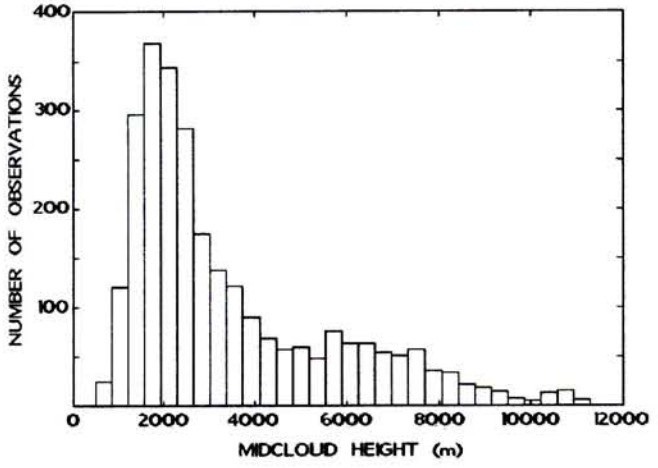

Fig. 4. Midcloud histogram Dumont D'Urville, 1989; midcloud is derived as first momentum of corrected backscattering profile. Clouds in which total laser beam extinction occurred are not shown because midcloud is not defined.

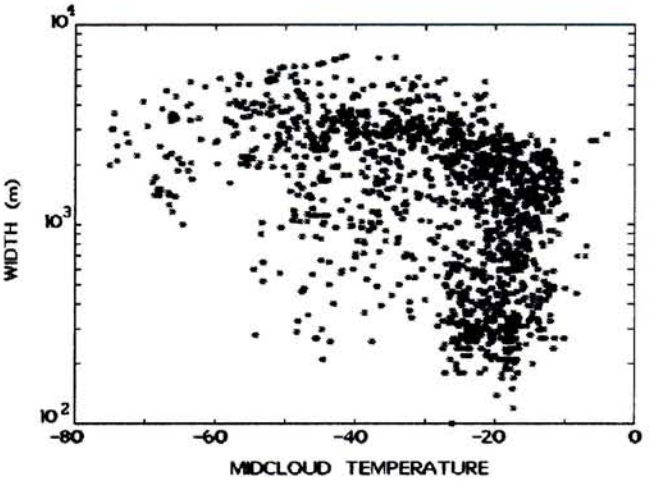

Fig. 6. Dumont D'Urville, 1989. Cloud width distribution. Clouds with unknown top are not shown.

distribution of cloud top and midcloud heights are present (Figures 4 and 5). As expected, most low-level clouds are trapped by the low-level inversion layer, while most cirrus clouds have their top just below the tropopause. Variations in the histogram shape are expected in the future if greenhouse forcing is really effective on cloud distribution.

The geometrical width of the cloud layers (Figure 6) is as interesting as base or top heights. At -20°C midcloud temperature a cluster of points shows layered clouds with a thickness of a few hundred meters. At the same temperature, other clouds form with widths of up to 2000 m (mostly clouds showing evidence of precipitation trails). Around -40°C midcloud temperature, clouds show maximum widths of 6000-7000 m (mean values around 3000 m). Higher clouds are thinner because their vertical extent is limited by the tropopause. A similar behavior with temperature has been obtained for midlatitude cirrus by *Platt* [1987] (with a maximum mean width of 3000-4000 m for winter midlatitude cirrus) and by J. Winkler (personal communication, 1992).

To establish the usefulness of midcloud temperature as an abscissa to plot high cloud quantities, an investigation was made to assess the temperature differences between the base and top heights of DDU clouds. In Figure 7 such a difference is plotted versus midcloud temperature. Several high clouds show differences up to 30°÷50°C so that in such cases, midcloud temperature is a rather ambiguous quantity. It is to be noted that most of these geometrically thick cold clouds show a constant optical depolarization through the whole profile, indicating no dramatic changes in the microphysical structure when cloud temperature is lower than -40°C.

From an overview of other lidar high-cloud measurements [*Dowling and Radke*, 1990] it appears that geometrically thicker high clouds have been detected in DDU. This difference could arise from real physical differences and/or from different definitions of cloud base. It should be stressed that cloud base is not evident in many precipitating clouds observed in DDU. The definition we used for cloud base includes lidar-evident precipitation trails.

Cloud base, top and midcloud heights are not fully satisfactory to specify the vertical shape of the cloud for

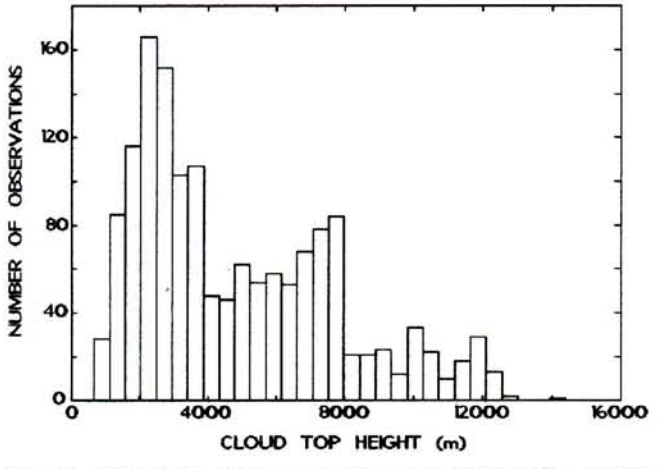

Fig. 5. Cloud top histogram Dumont D'Urville, 1989; clouds in which total laser beam extinction occurred are not shown.

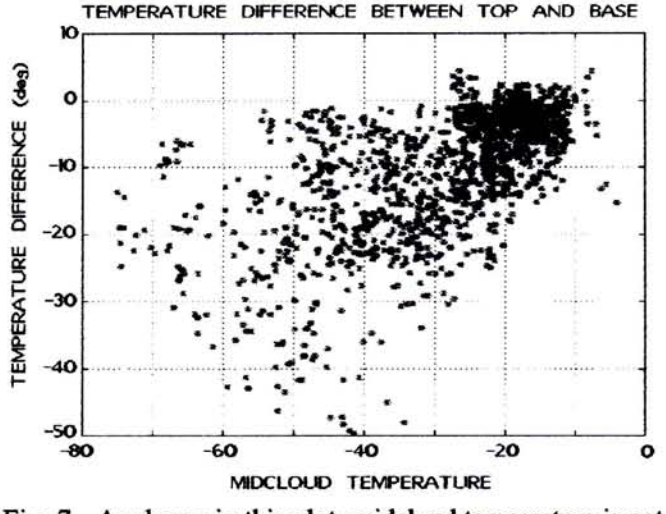

Fig. 7. As shown in this plot, midcloud temperature is not always a good axis to plot high-cloud characteristics, being as large as 40°-50°C in Dumont D'Urville, 1989.

radiative transfer computing. A geometrically thick cloud could be mostly composed of precipitation trails, while the major radiative layer could be much thinner and displaced far from midcloud. To partially overcome such difficulties, for each 30-min-averaged cloud signal the first three moments of the vertical distributions of $\beta_A(z)=\beta p_A(z)+\beta s_A(z)$ and Dep1 have been computed. Distribution moments are defined by

$$M_1 = \frac{\int \beta_A(z)\, z\, dz}{\int \beta_A(z)\, dz} \qquad (10)$$

and for $n > 1$

$$M_n = \frac{\int \beta p_A(z)\, (z-M_1)^n\, dz}{\int \beta p_A(z)\, dz} \qquad (11)$$

(integration limits are cloud base and top)

The first moment (M_1) of $\beta_A(z)$ is defined as midcloud. The second moment (M_2) is related to cloud thickness, being the square of the standard deviation of the Gaussian fit of the backscattering profile. The third moment (M_3) is related to the asymmetry of $\beta_A(z)$ with respect to the midcloud height. The asymmetry coefficient of a distribution is defined as $M_3/(M_2^{3/2})$. It is zero for clouds symmetrical around midcloud (e.g., Gaussian profile), positive for clouds whose $\beta_A(z)$ profile is sharper at the base than at the top, while it is negative for clouds with sharp tops (e.g., Ac clouds with virga). In Figure 8 the asymmetry coefficient of DDU clouds is plotted as a function of midcloud temperature. Most values are close to zero (almost symmetrical profile) with a mean around +0.5. Large negative values are more common for temperatures higher than -30°C, in agreement with those observed by *Platt* [1987] for cirrus. In Figure 8 , many points with strong negative asymmetry, above -40°C, are due to midlevel clouds precipitating ice.

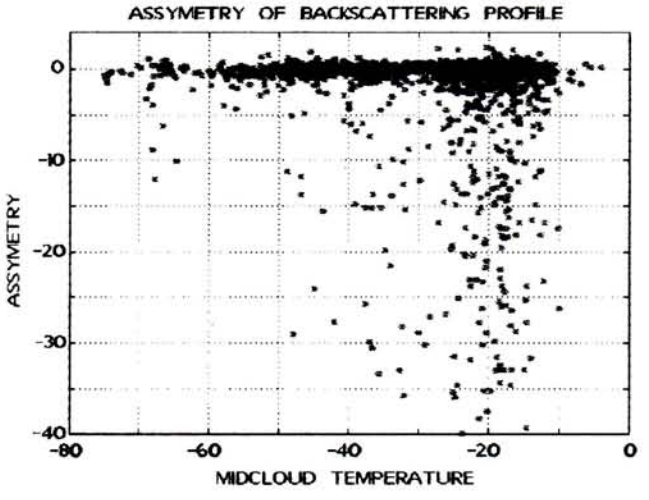

Fig. 8. Asymmetry factor (see text) of backscattering vertical profile, Dumont D'Urville 1989. Negative asymmetry means clouds with top sharper than base and vices.

5. THE 532-NM EXTINCTION AND BACKSCATTERING STATISTIC

The variations in cloud mean optical properties as a consequence of changes in temperature and humidity is a stimulating topic for all climate modelers. So far, the cloud models used in GMCs are still too primitive; several attempts, both theoretical and experimental, have been made to improve the parameterization of cloud sensitivity to climate changes.

A contribution of the present paper to this topic is the temperature trend of visible extinction. The values of mean extinction obtained for each 30-min average of DDU clouds are shown in Figure 9.

Clouds with optical thicknesses larger than 3 have not been represented because of the unreliability of the extinction, backscattering, and k parameter computed values. Stratocumulus cloud optical depth is generally bigger than 5, therefore most DDU low clouds are not represented in these plots. Anyway, useful information emerges for midlevel and high clouds.

A positive general trend of extinction with temperature is evident as already observed by *Platt and Harshvardhan* [1988] and computed by *Heymsfield and Platt* [1984] for high clouds.

Absolute extinction values for high DDU clouds are about 1 order of magnitude lower than those simulated by *Wright et al.* [1975], lower by 50% with respect to *Heymsfield and Platt* [1984], but in good agreement with simulations of *Takano and Liou* [1989], even if many optically thinner clouds are present in DDU data.

Extinction data points of DDU high clouds (midcloud temperature below -30°C, corresponding to about z > 4000 m) are plotted in Figure 10. A least squares fitting has been performed by using the formula

$$\sigma(T) = \exp[0.029\ T - 7.4535] \qquad (12)$$

with T in °C.

A comparison between DDU high-cloud extinction data with the cirrus extinction, measured by *Platt and Harshvardhan* [1988] at 11 μm and scaled to the visible

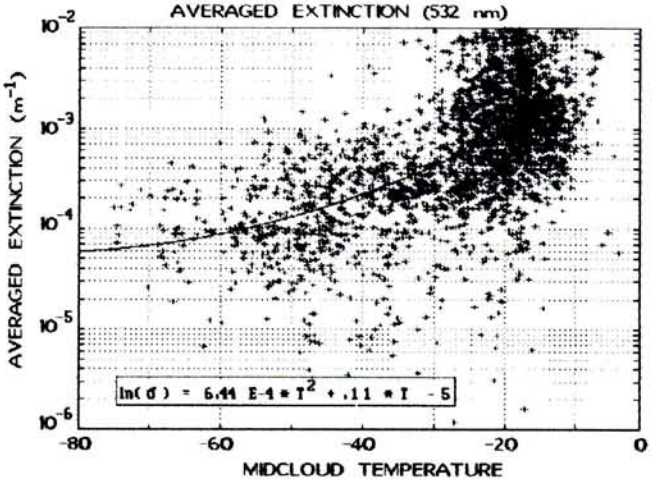

Fig. 9. Averaged extinction in Dumont D'Urville, 1989; data showing extinction below 1÷2E-5, affected by big processing errors, are not reliable. A fitting function $\sigma = \exp(-5.04 + 0.1098\ T + 0.0006\ T^2)$ is reported; having shown not clouds with optical depth > 3, such function is valid only up to about -20°C.

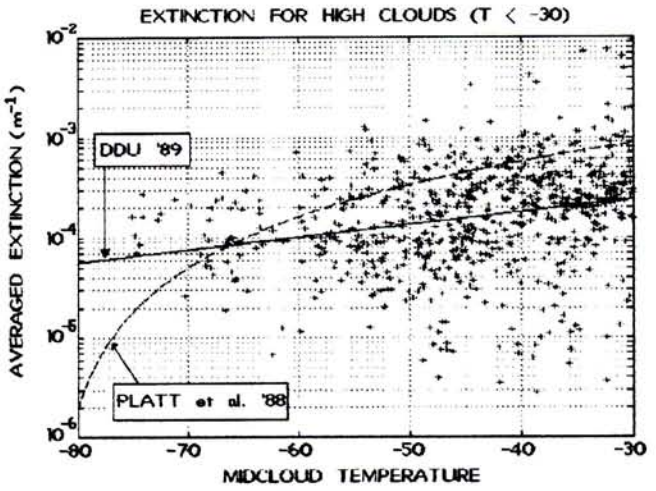

Fig. 10. Same plot as Figure 16 but limited to clouds colder than -30° (z > 4000 m, high clouds). A fitting function of Dumont D'Urville data is reported (see text) with continuous line. A visible extinction curve (dotted) derived from midlatitude cirrus infrared data [*Platt*, 1988] is also shown.

region, is performed in Figure 10. For cirrus clouds *Platt and Harshvardhan* obtained the following function

$$\sigma(T)=3.2E\text{-}7\ (T+82.5)^2 \qquad (13)$$

It was obtained by converting 11-μm IR absorption data to visible extinction by means of a constant factor of 2 (theoretically computed for ice crystals larger than 10 μm). The concentration of cirrus particles smaller than 20 μm is poorly known but seems to be at least as large as that of bigger particles [*Dowling and Radke*, 1990; *Heymsfield and Platt*, 1984]. The scaling of the extinction from IR to other wavelengths by means of a constant factor of 2 could therefore be unsatisfactory. This could partially explain the difference between the two fitting functions. Alternative explanations may lie in real physical differences between midlatitude and Antarctic high clouds or in different data analysis approaches.

Figure 11 shows optical depth of DDU clouds. Many clouds showing optical thicknesses $\delta <= 0.05$ (typical of subvisual clouds as observed by *Sassen et al.*, [1989]) are represented. As explained, relative errors are quite large for these clouds and can grow larger than 100 %.

It is interesting to note that even if extinction in high clouds may be 2 magnitudes smaller than in lower clouds, the difference in optical depth values is smaller as a result of the greater geometrical width of high clouds.

Figure 12 shows optical depth for high clouds (z > 4000 m, corresponding to about -30°C); a fitting function

$$\delta = \exp\,[0.0284\ T + 0.211] \qquad (14)$$

is represented. Optical depth magnitudes for high clouds are in the same range as observed by other lidar groups [*Notari*, 1990].

Two parameters of interest for climatic models are the extinction sensitivity factor

$$f_\sigma(T)=(1/\sigma)(d\sigma/dT) \qquad (15)$$

and the optical depth sensitivity factor

$$f_\delta(T)=(1/\delta)(d\delta/dT) \qquad (16)$$

Such parameters describe the trend of relative changes in σ and δ with temperature increase [*Platt and Harshvardhan*, 1988].

Figure 13 shows a comparison of visible extinction sensitivity factors as obtained from the fitting functions (12) and (13) for DDU and *Platt*'s data [1987]. Differences are substantial. DDU data show a constant sensitivity $f_\sigma(T)=0.029\ °C^{-1}$, converging to that of *Platt and Harshvardhan* [1988] at higher temperatures. The optical depth sensitivity factor derived from DDU data is again a constant

$$f_\delta(T)=0.0284\ °C^{-1}.$$

Figures 14, 15, and 16 show, respectively, the averaged, integrated backscattering coefficients and R-1 (excluding clouds with optical depth bigger than 3).

6. THE 532-NM OPTICAL DEPTH/INTEGRATED BACKSCATTERING PARAMETER (k)

The single-scattering extinction/backscattering ratio k' (equation (3)) is a number-density independent quantity; k'

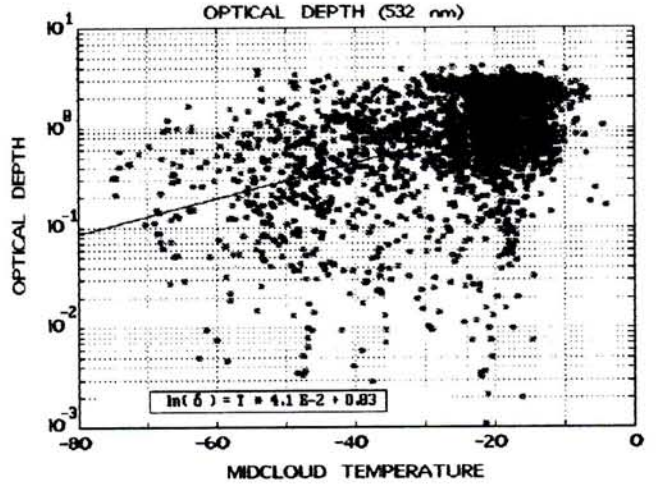

Fig. 11. Optical depth, Dumont D'Urville, 1989; values below 5E-2 are affected by a relative error > 100% .

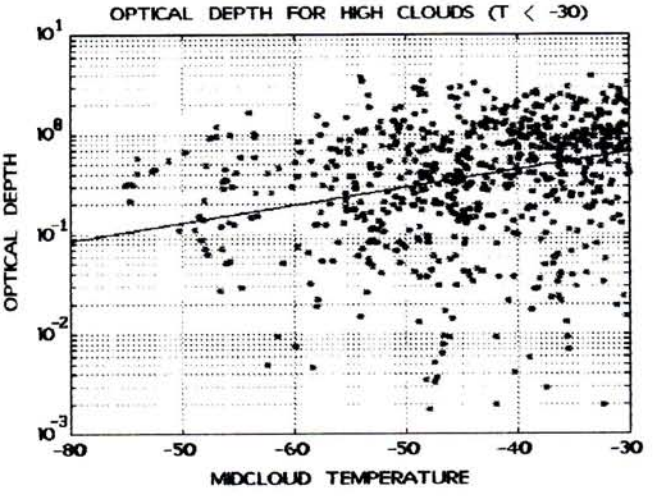

Fig. 12. Optical depth as in Figure 11 but limited to high-clouds only.

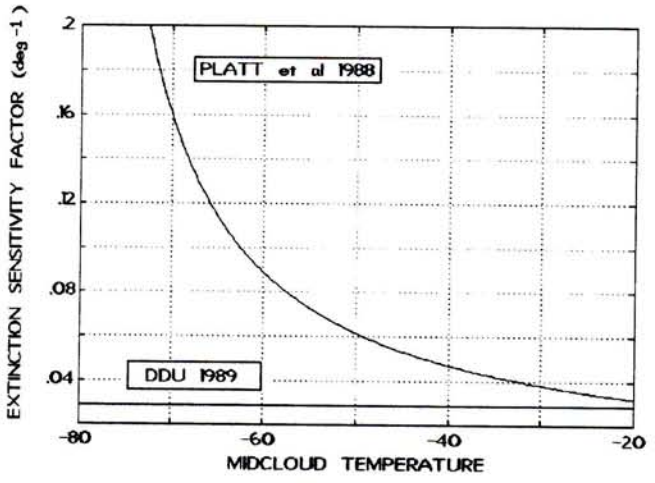

Fig. 13. Extinction sensitivity factor (see text, equation (14)) obtained from Dumont D'Urville data (dotted) and by *Platt* [1988] on midlatitude cirrus clouds. Y units are °C^{-1}.

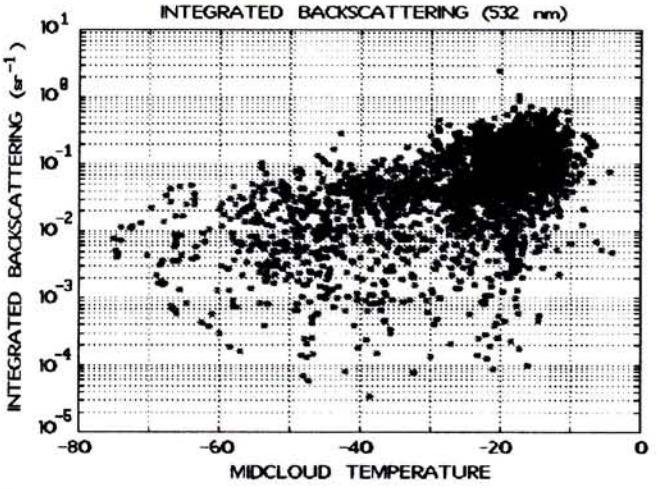

Fig. 15. Integrated backscattering, Dumont D'Urville, 1989.

is related to the shape of the single-scattering phase function of the scattering media. In optically thin clouds where single-scattering approximation ($\alpha=1$) is almost valid, the lidar-observed k (k= optical depth/integrated backscattering as from equation (3)) is equal to k'.

High values of k' (k'>20) are known both in the case of preferential forward scattering, typical of particles larger than the wavelength, and in the case of particles whose size is close to the wavelength, like stratospheric aerosols [*Pinnick et al.*, 1980; *Dubinsky et al.*, 1985; *Parameswaran et al.*, 1991].

For wavelengths up to about 1 μm, water clouds show a relatively constant value of k'. This is due to the absence of absorption and to the presence of spherical particles much greater than the wavelength. Several theoretical and experimental studies give an almost constant value of k' when varying the droplet density and size distribution: *Carrier et al.* [1967], $k'_{488nm}=16$, $k'_{1060nm}=22$ (theoretical computation); *Derr* [1980], $k'_{275nm}=16.3\pm15\%$, $k'_{1060nm}=18\pm15\%$ (theoretical computation on many selected water cloud types); *Pinnick et al.* [1983]: $k'_{632nm}=17.7$ (experimental); *Sassen and Lou* [1979]: $k'_{632nm}=25\div30$ (experimental); and *Dubinsky et al.* [1985]: $k'_{514nm}=20\div23$ (experimental with 2 to 6-μm mean radius droplets).

Ice clouds and mixed phase clouds generally show higher values of k' as result of the presence of big nonspherical particles with a typical forward scattering diagram. The relationship between the k' and the crystal habit or size is ambiguous. A short review of the values obtained for k is here reported: *Sassen and Lou* [1979]: $k'_{632nm}=120$ (small plates and columns) in cloud chamber; *Sassen* [1978], $k'_{632nm}=30$ (complex crystals), $k'_{632nm}=48$ (spatial crystals), and $k'_{632nm}=300$ (small "simple" crystals); *Platt* [1973], $k'_{694nm}=38\div66$ in cirrus cloud measurements (lidar plus radiometer); *Platt* [1987] (same method), $k'_{694nm}=40\div80$ with temperature, seasonal and latitudinal variations; *Platt et al.* [1989] (same method), $k'_{694nm}=31\div89$; and *Notari et al.* [1990] $k'_{532nm}=30\div80$ in cirrus clouds. Simulations of Takano reported by *Sassen et al.* [1989] give k'=38 for thin plates, k'=116 for thick plates, and k'=26 for long columns. Several observations of cirrus clouds showing very low k' (close to that of water clouds) have been carried out by *Platt* [1987] with 694-nm lidar plus radiometer. Such unexpected results have been associated with the presence of horizontally oriented plates.

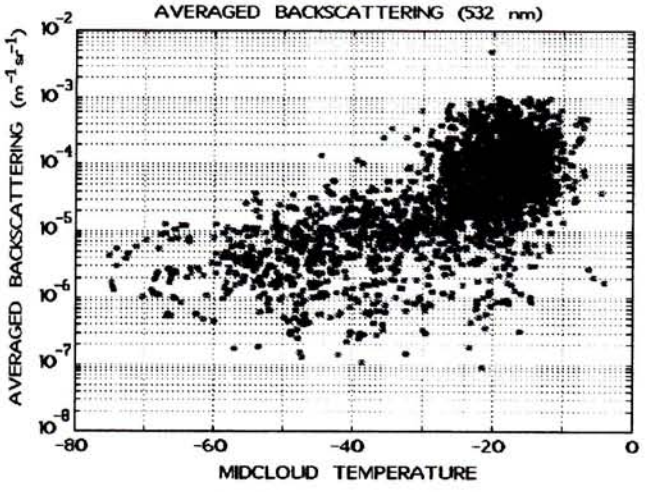

Fig. 14. Averaged backscattering coefficient in Dumont D'Urville, 1989. Points below 1÷3E-7 are not reliable.

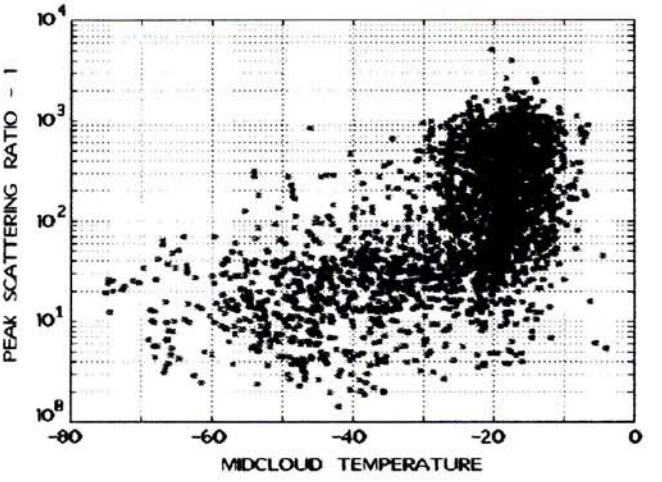

Fig. 16. Peak R-1; Dumont D'Urville clouds with optical depth $\delta > 3$ are not shown.

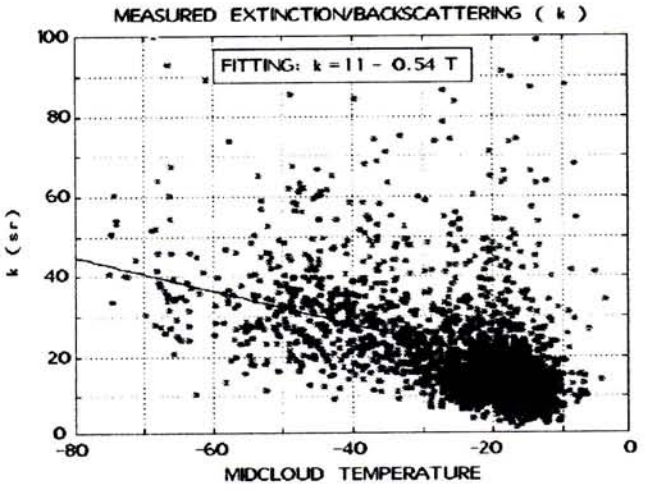

Fig. 17. Extinction/Backscattering ratio k for Dumont D'Urville clouds; the fitting A is obtained with all the clouds, while fitting B is obtained with all clouds dense enough to give completely meaningful k values.

The values of k obtained for all processed DDU clouds by equation (3) are shown in Figure 17, together with a linear least squares fit. Water clouds generate a cluster in the plot and show a mean k around 15, smaller than values typically obtained by the other authors. This is mainly due to multiple scattering, as shown in Figure 18, where k values are plotted versus optical depth for water clouds ($T > -30$ and peak Dep2 $< 25\%$) for which an almost constant k' ($k' \approx 18$) is expected from single scattering. The negative trend of k corresponds to a decrease of α from 1 (single scattering) to $\alpha = 0.83$ for $\delta = 2.5$. This means a multiple-scattering induced error of about $-(10\delta)\%$ on extinction and optical depth in thick water clouds, and an approximate relationship for multiple scattering factor $\alpha \approx 1 - \delta/10$.

A similar estimation is not possible for ice clouds, being k theoretically unknown, but plots of k obtained by selecting thin high clouds only ($\delta < 0.5$) show the same trend as Figure 17, suggesting a negligible multiple-scattering error in such clouds. The values of k for mixed phase clouds are close to those obtained for water clouds. In fact, the correction for the extinction of a lidar backscattering profile is sensitive to the part of the mix phase cloud showing greater backscattering, generally the water part which therefore has a predominant weight in the k estimation. As a consequence, mix phase clouds cannot be distinguished from water clouds on the basis of the k value only, an analysis of the depolarization profile being necessary.

The points with temperatures lower than -40°C (Figure 17) showing small k values could derive from horizontally oriented plate crystals (see depolarization paragraph).

The trend of k with temperature for DDU high clouds is in agreement with *Platt* [1987]. Figure 19*a* shows $K = 4\pi/k$ (for homogeneity with *Platt*'s [1987] data, plotted in Figure 19*b*, where $K\alpha/(2\alpha p)$ is proportional to K by the multiple scattering factors α (for DDU) and αp (for Platt). In both graphs a change in K between -30° and -40° is clear. Such behavior could be due to a

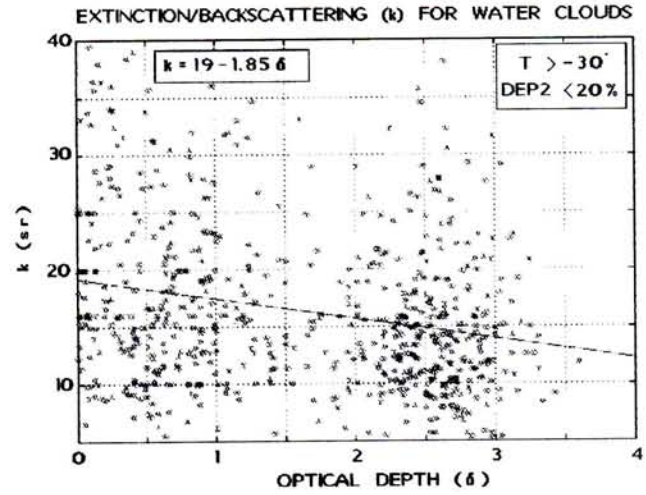

Fig. 18. Extinction/Backscattering ratio k of clouds warmer than -30°C and with peak depolarization smaller than 20%. The majority of such clouds are composed of liquid water with known k'.

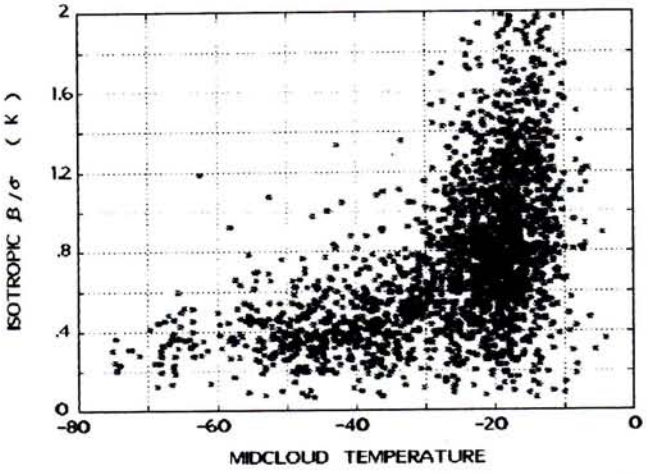

Fig. 19*a*. Isotropic backscattering/extinction ratio $K = 4\pi/k$ from Dumont D'Urville 1989 data (from lidar data only).

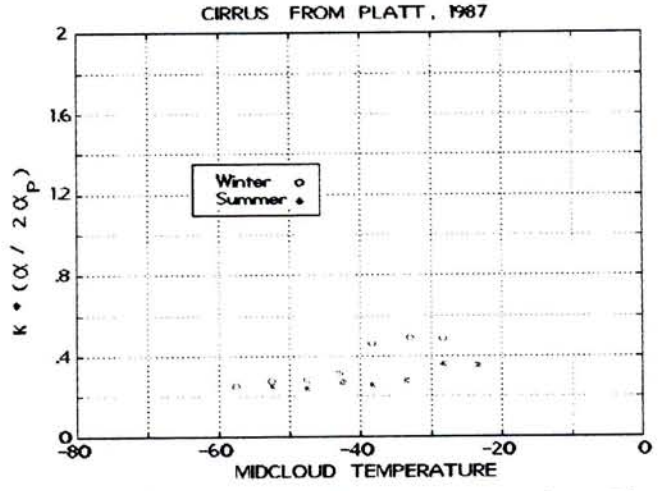

Fig. 19*b*. Temperature trend of $K\alpha/(2\alpha p)$ from *Platt* [1987] as obtained by means of lidar+radiometer. Such quantity is proportional to the isotropic backscattering/extinction K (see Figure 19*a*) by a factor $\alpha/2\alpha p$, dependent on the multiple scattering factors of the two lidars.

change in crystal habit and/or size distribution with temperature.

7. THE 532-NM DEPOLARIZATION DATA

The depolarization of linearly polarized laser light by means of aerosol particles is a helpful parameter in the investigation of the physical phase of water in clouds [*Sassen*, 1991*a*].

It is generally accepted that neglecting the multiple-scattering contribution, water droplets show low depolarization values (less than 20%), while ice particles generally show higher values, ranging between about 20 up to 80 % [*Pal and Carswell*, 1973; *Derr et al.*, 1976; *Sassen*, 1976; *Platt*, 1977].

Two definitions of the depolarization (Dep1 and Dep2) have been used in DDU cloud analysis. The main difference between Dep1 and Dep2 is that the latter is computed on the basis of cloud backscattering profiles (β_{PA} and β_{SA}, taking away the molecular profile from the lidar returns. A disadvantage is that the accuracy of Dep2 depends on the fitting and on the reliability of the molecular atmosphere model. On the other hand, Dep1 is meaningless for very thin clouds whose backscattering has the same magnitude of the one due to the molecular atmosphere. The depolarization averaged through the whole cloud profile is a meaningful value only for homogeneous clouds, while peak values could be related either to the ice part of mixed phase clouds or to the depolarization peak induced by multiple scattering in water clouds. Both averaged and peak depolarization values are, from this point of view, incomplete data if not given together with β_A and depolarization vertical profiles.

The data set presented in this work includes ice, water, and mixed phase clouds. The values of Dep1 and Dep2 are shown in Figures 20, 21, 22, and 23. Due to subtraction of molecular contribution, Dep2 shows more constant peak values than Dep1 in high clouds.

Figure 22 shows that Dep2 is quite constant (15-20%) below -30°C, with a slow linear growth toward lower temperatures. The trend is similar to the one observed by *Platt* [1987] for tropical cirrus.

DDU high clouds show depolarization values smaller than those normally observed in midlatitude cirrus [*Platt*, 1987], while similar low values have been observed in cloud chambers [*Sassen and Lou*, 1979] and in cold cirrus layers (around -60°C) [*Sassen et al.*, 1989].

High clouds showing depolarization lower than 20% are frequently interpreted as anomalous cases due to small subspherical ice particles, supercooled droplets, or horizontally oriented plates. The wide occurrence of such low values in DDU clouds indicates a more general pattern, extending throughout the entire area below -30°C. The presence of large plates (200-300 μm) capable of showing horizontal orientation and low depolarization becomes improbable when increasing the height, as observed by *Heymsfield and Platt* [1984] and *Sassen* [1984]. Also, the presence of supercooled droplets becomes highly improbable with temperatures much lower than -40°C.

The relatively low depolarization of DDU high clouds could be explained by the presence of small ice particles. Little is known about the occurrence of nonspherical cirrus particles smaller than a few tens of microns [*Dowling and Radke*, 1990].

Depolarizations comparable with those observed in DDU high clouds have been obtained theoretically by *Asano* [1983] for small ice prolated spheroids (<2 μm at 532

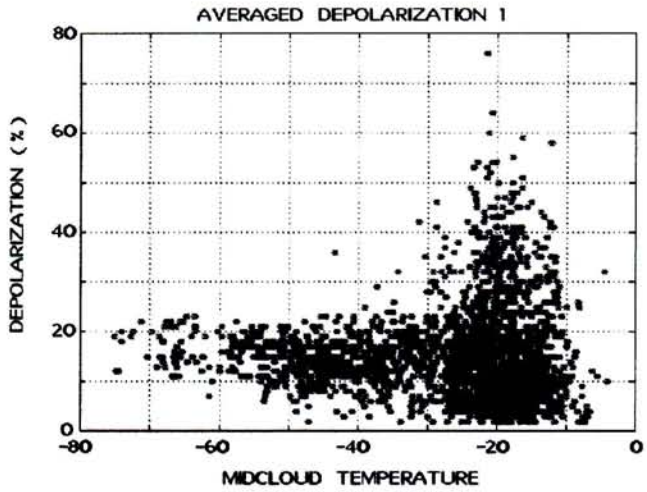

Fig. 21. Dumont D'Urville, 1989. Peak values of depolarization (Dep1).

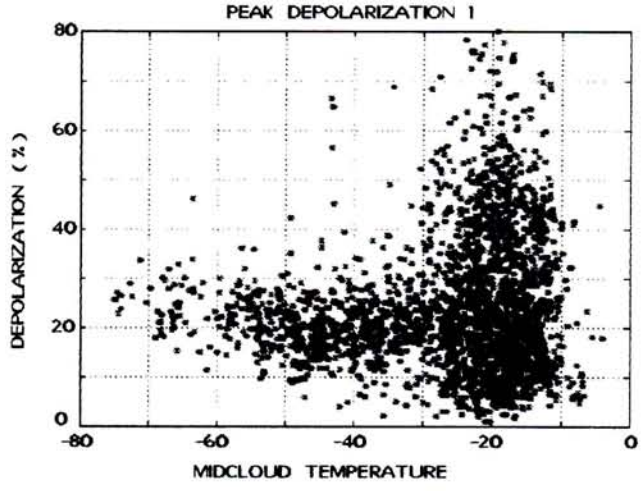

Fig. 20. Dumont D'Urville, 1989. Cloud-averaged depolarization ratio (Dep1) versus midcloud temperature; dispersion of Dep1 toward low values in high clouds is due to the dominating Rayleigh contribution to the parallel backscattering component.

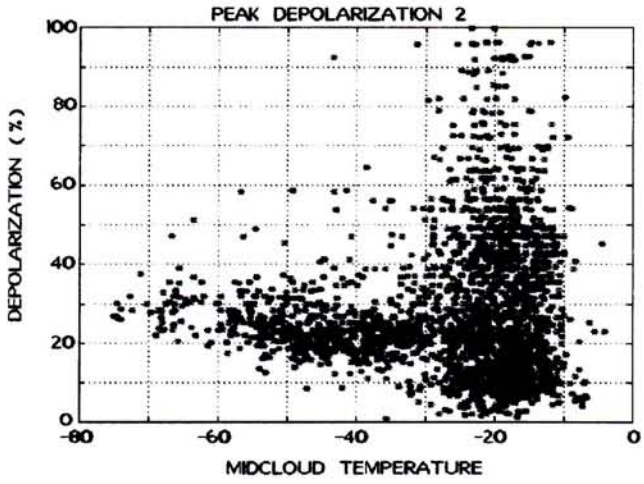

Fig. 22. Dumont D'Urville, 1989. Peak values of Dep2. For high clouds the dispersion of Dep2 values is smaller than that of Dep1 (Figure 28); this is due to the subtraction of the Rayleigh component.

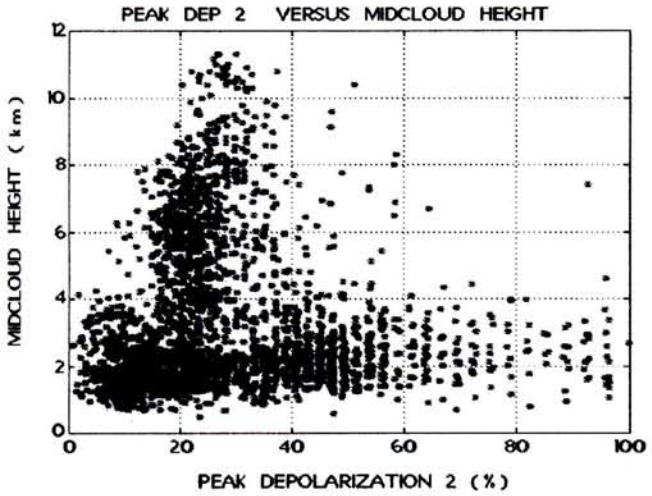

Fig. 23. Dumont D'Urville, 1989. Trend of the peak values of Dep2 with altitude.

nm) randomly oriented with their long axis on a plane. On the other hand the same reference shows that depolarizations from 10% (strongly prolated particles) up to 80% (slightly prolated particles) are expected, with nonlinear behavior regarding asphericity and size. Similar disappointing results are obtained by *Flesia et al.* [1992]. These works (related to particles of small size, accounting for only a part of cirrus cloud size distribution) show how ambiguous particle shape classification is on the basis of the depolarization, when not filled out by additional information.

Apart from the hypothesis of small particles, peak values of Dep2 around 20% are in agreement with those theoretically computed for three-dimensional randomly oriented bigger ice columnar crystals of various sizes [*Sun et al.*, 1989]. In the same reference, values of Dep2 of about 80% for randomly oriented plate crystals are reported, allowing a distinction between randomly oriented plates (or more complex crystals) and columns.

A few clouds at temperatures lower than -30°C show very low Dep2 (Figure 22). These points could be due either to supercooled droplets or to horizontally oriented plate crystals, while higher Dep2 peak values (up to 60% peak) below -40°C could arise from particles other than columns, like hexagonal plates. The occurrence of points with peak Dep2 > 100% could be explained by the presence of a strongly anisotropic medium, like that produced by large oriented plate crystals or by processing errors. In the region of Figure 22 warmer than -30°C, a cluster of points around 10% depolarization is due to liquid water-dominated clouds, while higher values are due to ice and mixed phase clouds. In this region optically thick clouds occur. In such cases, depolarization values can be strongly affected by multiple scattering, the effect depending on the field of view of the lidar and cloud penetration. Tests performed on thick stratocumulus showed that maximum multiple-scattering-induced depolarization was of about 20% at cloud top, so that larger values of dep2 are certainly due to ice presence.

Around -25°÷30°C midcloud temperature, a change in maximum peak depolarization values is evident, showing a change in crystal habit variety. A change from dominating columnar particles to plates or spatial crystals and aggregates occurs above -20°÷25°C in a cloud chamber [*Pruppacher and Klett*, 1985] and around -40°÷50°C in real cirrus, together with an increase of maximum particle size [*Heymsfield and Platt*, 1984]. The change depends upon water vapor availability and condensation history. Thick hexagonal plates have been observed more rarely in cirrus clouds below -40°C [*Heymsfield and Platt*, 1984; *Sassen*, 1991*b*] and trigonal crystals around -80°C [*Heymsfield*, 1986].

A change of crystal habit is supposed to occur in our data at about -25°÷30°C, if we accept that Dep2 values around 20% are mainly connected to columnar ice crystal presence rather than to size distributions dominated by small nonspherical particles.

It is stimulating to verify that such an abrupt change in depolarization is coincident to the apparition of mixed phase clouds above -25°÷30°C. In Figure 24 the correlation coefficient between Dep1 and backscattering vertical profiles is shown. The coefficient is close to 1 in clouds where backscattering and depolarization profiles have similar shapes (uniform composition) and becomes negative toward -1 when depolarization and backscattering profiles are shifted (separate layers of ice and water or layers with different ice crystal habit). It is evident that most mixed phase clouds occur above -25°÷30°C.

The correlation coefficient gives no information about the relative position of the ice and water layers. To assess this, in Figure 25 the vertical shift between the first momentum of depolarization and backscattering profiles and the temperature is plotted. Negative shifts down to -1000 m (ice layers under water layers) occur in most clouds warmer than -25°÷30°C. Such clouds have often been observed by the naked eye as ice precipitating altocumulus. The -25°÷30°C boundary does not seem to be related either to stable temperature inversions or to humidity changes above DDU.

8. CONCLUSIONS

In this study a statistical overview of 1 year of lidar observations of Antarctic coastal clouds has been performed, taking into account all of the optical and geometrical quantities retrievable from lidar and available balloon soundings.

Lidar data processing involved a modified *Klett* [1981] inversion method developed at IROE and tested for various error sources. Thirty-minute lidar data averages have been considered as single cloud observations.

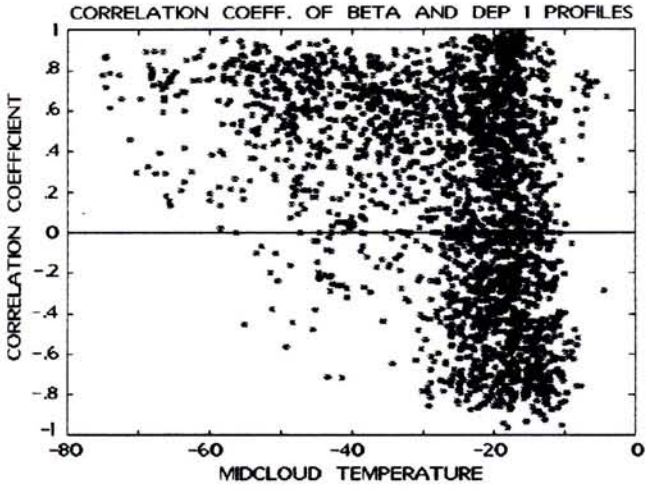

Fig. 24. Dumont D'Urville, 1989. Temperature dependency of correlation coefficient between Dep1 and backscattering profiles. Positive values close to 1 indicate clouds with uniform composition, negative values close to -1 highly layered mixed phase clouds.

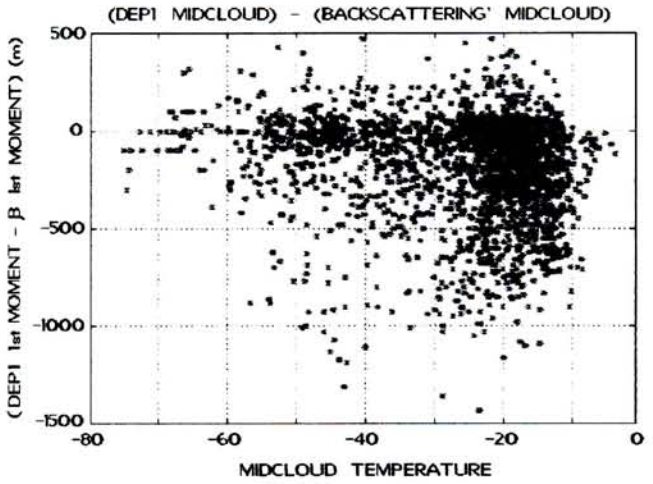

Fig. 25. Dumont D'Urville, 1989. Temperature dependency of the shift between the medians (M1) of Dep1 and backscattering profiles; negative shift reveals ice-precipitating water clouds.

Statistics of cloud base, top, and midcloud as obtained by means of lidar have been produced. Results show that DDU high clouds are relatively thicker (mean thickness 3000 m) than those observed at midlatitudes. Because of the large vertical extent of such clouds, temperature difference between base and top can be as high as 40°-50°C. A typical uniformity of depolarization in such cold clouds has been noted, suggesting no dramatic changes of crystal habit or size distribution below -40°C.

On the average, high clouds have their top below 8000 m (tropopause topped), but many clouds have been observed above the tropopause during winter months when the tropopause inversion is weak. Most low-level stratified clouds have their top around 2500 m (determined by a stable inversion layer). Low and midlevel clouds dominated 1989 DDU data.

Clouds at temperatures above -30°C often show strong negative asymmetry of the vertical backscattering profile due to the occurrence of precipitation trails (often observed by naked eye in DDU Ac clouds). Precipitation trails have also been detected in some high-level clouds.

Statistics of 1 year's Antarctic cloud extinction and optical depth based on lidar and radiosondes have been produced as a contribution to cloud modeling. Results show a wide data dispersion with an evident positive trend of averaged extinction (σ) and optical depth (δ) with midcloud temperature in high and midlevel clouds. Such a trend allowed the computation of temperature sensitivity parameters related to the cloud's σ and δ. Results show a substantial constancy of such parameters with midcloud temperature. The strong temperature trend of extinction is less evident in optical depth because cold optically thinner clouds are geometrically wider.

Midcloud temperature dependency of averaged backscattering, integrated backscattering, and peak scattering ratio have been plotted as a contribution to cloud modeling and for the improvement of lidar simulation programs.

Extinction versus backscattering ratio k have been computed by means of lidar data only. A negative trend with midcloud temperature has been assessed, as already observed by other authors, but with k absolute values relatively smaller; k is relatively linear with midcloud temperature. When $4\pi/k$ instead of k is plotted, it shows a behavior similar to that observed by *Platt* [1987]. The errors induced by multiple scattering on retrieved extinction, optical depth, and k values are smaller than 30% in optically thick ($\delta > 2$) low clouds and become apparently negligible in high clouds.

A depolarization trend with midcloud temperature has been obtained, showing a constancy of depolarization below -30°C. In such regions the depolarization is lower than generally observed in midlatitude cirrus clouds, being in the range Dep2 = 15÷30% with a slight negative trend with temperature. Below -30°C only a few clouds show Dep2 peak values larger than 30%, suggesting a constancy of crystal habit in such a region. The presence of columnar crystals or small ice particles is suggested. A change of crystal habit (or size) around -25°÷30°C is evident in our data. Above such temperatures, Dep2 peak data split into two clusters. The first with values lower than 20%, typical of water clouds, and the second, perhaps due to ice crystals of complex shape, around 40-60%.

Scattered points with Dep2 even higher than 100% are supposed to be due to strongly anisotropic media like that produced by oriented plates.

Above -25°÷30°C, mixed phase clouds have been frequently recognized in DDU data by correlating backscattering and depolarization profiles. Such clouds have been identified as ice-precipitating midlevel clouds.

An attempt to correlate horizontal advection as deduced from balloon soundings and various optical quantities has been attempted, finding no significant differences in optical properties of clouds having different air mass origins.

Acknowledgements. This study has been developed in the frame of an Italian-French cooperative project between PNRA (National Program for Antarctic Research, Italy) and TAAF (Terres Australes Antarctiques Françaises, France). The authors are very thankful for the friendship and the help received by all the people of EPF (Expeditions Polaires Francaises) working in DDU for the expeditions TA39, TA40, and TA41. We wish to thank the local meteostation for the meteorological data used in this work. We also wish to thank Enrico Palchetti, Lionello Zuccagnoli, Francesco Castagnoli, Valerio Venturi (for the lidar station design and assemblage), and Vincenzo Maria Sacco (for the acquisition software). We are very grateful to the whole ECLIPS community for the stimulating workshops which were fundamental in the development of the methodology used in this work.

REFERENCES

Asano, S., Light scattering by horizontally oriented spheroidal particles, *Appl. Opt.*, *22*, (9), 1390-1396, 1983.

Carleton, A.M., Monthly variability of satellite-derived cyclonic activity for the southern hemisphere, *J. Climatol.*, *1*, 21-38, 1981.

Carrier, L.W., G.A. Cato, K.J. von Essen, The backscattering and extinction of visible and IR radiation by selected major cloud models, *Appl. Opt.*, *6* (7), 1209-1216, 1967.

Cess, R.D., et al., Intercomparison and interpretation of climate feedback processes in 19 atmospheric general circulation models, *J. of Geophys. Res.*, *95*(10), 16,601-16,615, 1990.

Derr, V.E., Estimation of the extinction coefficient of clouds from multiwavelength lidar backscattering measurements, *Appl. Opt.*, 19(14),*15*, 2310-2315, 1980.

Derr, V.E., N.L. Abshire, R.E. Cupp and G.T.

McNice, Depolarization of lidar returns for virga and source cloud, *J. Appl. Meteorol.*,*15*,1200-1203, 1976.

Dowling, D.R., and L.F. Radke, A summary of physical properties of cirrus clouds, *J. of Appl. Meteorol.*, *29*, 970-978, 1990.

Dubinsky, R.H., A.I. Carswell, S.R. Pal, Determination of cloud microphysical properties by laser backscattering and extinction measurements, *Appl. Opt.24*, 1614, 1985.

Experimental Cloud Lidar Study (ECLIPS), *Rep. WCRP/CSIRO Workshop, WMO/TD-251*, 1988.

Fernald, F.G., Analysis of atmospheric lidar observations: some comments, *Appl. Opt.*, *23*(5), 1984.

Flesia, C., A. Mugnai, L. de Schoulepnikoff, and L.Stefanutti, Lidar depolarization by nonspherical particles: Potential for polar stratospheric clouds characterization, *Appl. Opt.*, in press, 1992.

Graeme L., J. Stephens and T.J. Greenwald, The Earth's radiation budget and its relation to atmospheric hydrology, 2, Observations of cloud effects, *J. of Geophys. Res.*, *96*(D8), 15, 325-340, 1991.

Heymsfield, A.J., and C.M.R. Platt, A parameterization of the particle size spectrum of ice clouds in terms of the ambient temperature and the ice water content, *J. Atmos. Sci.*,*41*(5), 846-855, 1984.

Heymsfield, A.J., Ice particles observed in a cirriform cloud at -83 C and implications for PSC, *J. Atmos. Sci.*, *43*(8), 851-855, 1986.

Klett, J.D., Stable analytical inversion solution for processing lidar returns, *Appl. Opt.*, *20*(2), 211-220, 1981

Klett, J.D., Lidar inversion with variable backscattering/extinction ratio, *Appl. Opt.*, *22*(4), 1638-1643, 1985

Mitchell, J.F.B., C.A. Senior, W.J. Ingram, CO_2 and climate: a missing feedback?, *Nature, 341*, 132-134, 1989.

Morandi, M., A complete procedure for inverting backscattering lidar returns. *Res. Rep. RR/GCF/92.11*, Ist. di Ric. Onde Elettromagn., 1992.

Notari, A., U.N. Singh, T.D. Wilkerson, and W.C. Braun, Optical properties of high clouds, Optical remote sensing of the atmosphere, *Tecn. Dig. Ser.*, *4*, 210-212, 1990.

Pal, S.R., and A.I.Carswell, Polarization properties of lidar backscattering from clouds, *Appl. Opt.* 12, 1530-1535, 1973.

Parameswaran, K., K.O. Rose, and B.V. Krishna Murthy, Relationship between backscattering and extinction coefficients of aerosols with application to turbid atmosphere, *Appl. Opt.*, *30*(21), 3059-3071, 1991.

Pinnick, R.G., S.G. Jennings, and P. Chylek, Relationships between extinction, absorption, backscattering and mass content of sulfuric acid aerosols, *J. Geophys. Res.*, *85*(C7), 4059-4066, 1980.

Pinnick, R.G., S.G. Jennings, P. Chylek, C. Ham, and W.T. Grandy, Backscattering and extinction in water clouds, *J. Geophys. Res.*, *88*(C11), 6787-6796, 1983.

Platt, C.M.R., Lidar and radiometric observations of cirrus clouds, *J. Atmos. Sci.*, *30*, 1191-1204, 1973.

Platt, C.M.R., Lidar observation of mixed phase altostratus clouds, *J. Appl. Meteorol.*, *16*, 339-345, 1977.

Platt C.M.R., Remote sounding of high clouds, VI, Optical properties of midlatitude and tropical cirrus, *J. Atmos. Sci.*, *44*(4), 729-747, 1987.

Platt, C.M.R., N.L. Abshire, and G.T. McNice G.T., Some microphysical properties of an ice cloud from lidar observation of horizontally oriented crystals., *J. Appl. Meteorol.*, *17*, 1220-1224, 1978

Platt, C.M.R., and S. Harshvardhan, Temperature dependence of cirrus extinction: Implications for climate feedback, *J. Geophys. Res.*, *93*(D9), 11051-11058, 1988.

Platt, C.M.R., J.D. Spinhirne, and W.D. Hart, Optical and microphysical properties of a cold cirrus cloud: Evidence for regions of small ice particles, *J. Geophys. Res.*, *94*(D8), 11151-11164, 1989.

Pruppacher, H.R., D.J. Klett, Clouds and precipitation, D. Reidel, Noerwell, Mass., 1985.

Rind, D., E.W. Chiou, W. Chu, J. Larsen, S. Oltmans, J. Lernier, M.P. McCormick, L. McMaster, Positive water vapor feedback in climate models confirmed by satellite data, *Nature, 349*, 500-503, 1991.

Sacco, V.M., F. Castagnoli, M. Morandi, and L. Stefanutti, Elastic backscattering lidar system for atmospheric measurements in Antarctica, *Opt. and quantum Electron.*, *21*, 215-226, 1989.

Sassen, K., Polarization diversity lidar returns from virga and precipitation. *J. Atmos. Sci. 34*, 1444-1457, 1976.

Sassen, K., Backscattering cross sections for hydrometeors: Measurements at 632 nm, *Appl. Opt. 17*, 804-806, 1978.

Sassen, K., Deep orographic Cloud structure and composition derived from comprehensive remote sensing measurements, *J. Clim. Appl. Meteorol.*, *23*, 568-583, 1984

Sassen, K. The polarization lidar technique for cloud research: a review and current assessment, *Bull. Am. Meteorol. Soc, 72*(12), 1991a.

Sassen, K., Corona-producing cirrus cloud properties derived from polarization lidar and photographic analyses, *Appl. Opt.*, *30*(24), 3421-3428, 1991b.

Sassen, K., and K.N. Lou, Scattering of polarized laser ligth by water droplet, mixed-phase and ice clouds, II, *J. Atmos. Sci.*, *36*, 852-861, 1979

Sassen, K., M.K. Griffin, G.C. Dodd, Optical scattering and microphysical properties of subvisual cirrus clouds, and climatic implications, *J. Appl. Meteorol.*, *28*, 91-98, 1989.

Schwerdtfeger, W., *Weather and climate of the Antarctic*, Elsevier Science, New York, 1984

Slingo, A., Sensitivity of Earth's radiation budget to changes in low clouds, *Nature, 343*, 49-51, 1990.

Stephens, G.L., and T.J. Greeenwald, The Earth's radiation budget and its relation to atmospheric hydrology, 2. Observation of cloud effect, *J. of Geophys. Res.*, 96, 15325-15340, 1991.

Sun, Y.Y., Z.P. Li, and J. Bosenberg: Depolarization of polarized light caused by high altitude clouds, 1, Depolarization of lidar induced by cirrus, *Appl. Opt.*, *28*(17), 1989.

Takano, Y., K.N. Liou, Solar radiative transfer in cirrus clouds, I: Single scattering and optical properties of hexagonal ice crystals, *J. Atmos. Sci.*, *46*(1), 3-19, 1989.

Wright, M.L., E.K. Proctor, L.S. Gasiorek, and E.M Liston, A preliminary study of air pollution measurement by active remote sensing tecniques, final report, NASA contract NAS1-11657, 1975.

M. Del Guasta, M. Morandi, and L. Stefanutti, Istituto Ricerca Onde Elettromagnetiche, CNR, Via Panciatichi 64, 50127 Firenze, Italy.

J. Brechet and J. Piquard, Expeditions Polaires Françaises, 47 Avenue du Marechal Fayolle, 75116, Paris, France.

(Received October 4, 1992;
revised May 5, 1993;
accepted May 28, 1993.)

JOURNAL OF GEOPHYSICAL RESEARCH, VOL. 98, NO. D10, PAGES 18,575–18,587, OCTOBER 20, 1993

One Year of Cloud Lidar Data From Dumont d'Urville (Antarctica) 1. General Overview of Geometrical and Optical Properties

MASSIMO DEL GUASTA, MARCO MORANDI, AND LEOPOLDO STEFANUTTI

Istituto Ricerca Onde Elettromagnetiche of CNR (Florence, Italy)

JACQUES BRECHET AND JACQUES PIQUAD

Expeditions polaires francaises, (Paris, France)

Tropospheric clouds play a major role in climate regulation but, so far, only a few long-term ground-based observations, devoted to the study of the cloud optical and radiative properties, have been carried out. In this work the statistics of 1 year of coastal Antarctic cloud lidar measurements (532 nm) are shown. Cloud macrophysical and optical parameters have been retrieved from lidar returns; radiosonde data allowed us to build statistics of such quantities in terms of cloud temperature. Information about the physical phase of water and ice crystal habit has been obtained from the depolarization and extinction/backscattering ratio; a change in crystal habit (and/or size) around -30 °C is evidenced by the depolarization versus temperature behavior. The extinction/backscattering ratio shows a negative trend with temperature, reflecting microphysical changes. Visible extinction shows wide data dispersion, but with a marked negative trend with temperature. The relative derivatives of extinction and optical depth with temperature have been computed, such quantities result quite constant with temperature.

1. INTRODUCTION

The difficulty in the realistic modelling of the Earth's climate is intrinsically related to the complexity of the studied system. The interactions connecting the "simple" components of atmosphere, ocean, crust and biosphere are little known, even from a qualitative point of view. For this reason, improvement of global circulation models (GCMs) needs a large amount of statistically valid empirical data to be used as a basic input. As a primary rough output, the sensitivity of GCMs to particular phenomena is assessed in order to address further research on the most important links of the chain. Clouds are one such topic, as their effect on the Earth's radiation budget is one of the main uncertainties of GCM outputs [*Cess et al.*, 1990; *Slingo*, 1990]. Actual cloud effect on radiation budget, as observed by satellite, shows strong seasonal and regional variations [*Stephens and Greenwald*, 1991] contributing to a mean surface cooling of about 18°C when compared to a cloudless Earth. Changes in microphysical or macrophysical cloud properties could modify this balance. GCMs predict a vertical and latitudinal change in water vapor distribution as a result of greenhouse gas increase [*Mitchell et al.*, 1989] (as confirmed by satellite data [*Rind et al.*, 1991]). Such models predict a change in cloud frequency, height and composition following greenhouse forcing.

Ground-based lidars working on a routine basis could give useful information for GCM cloud parameterization. A network of such instruments can follow possible changes of macrophysical properties of clouds, giving helpful information about their microphysics. Comparison between lidar and satellite cloud data can largely improve cloud algorithms for satellite data processing. In this spirit, part of the data set presented in this work has been collected in the frame of the *Experimental Cloud Lidar Pilot Study (ECLIPS)* [1988]. Data refer to the Antarctica, a region insufficiently researched in tropospheric studies.

A depolarization backscattering lidar was operated in 1989 and 1990 at the base of Dumont d'Urville (DDU), located on an island a few kilometres off the coast of Antarctica (66° S, 140° E). Cloud data were collected, on a routine basis, 24 h/d. The laser was operated with a 1 pulse/min repetition rate and 10-min averaged profiles were acquired. During the ECLIPS campaigns the laser was operated with a 6-pulse/min repetition rate, while signatures averaged over 1 min were acquired.

Daily balloon soundings and three hourly ground-based meteorological observations are available. Continuous video recording of clouds, LW, and SW radiometric data (wideband - wide-angle PIR and PSP radiometers) and meteorological maps are also available.

2. METHOD FOR INVERTING LIDAR DATA WITH RESPECT TO THE OPTICAL PARAMETERS.

The main characteristics of the lidar system [*Sacco et al.*, 1989] are as follows: A frequency doubled Nd:YAG laser is used as a transmitter. The pulse energy is about 400 mJ at 532 nm with a 10 pps maximun repetition rate and the divergency is about 0.5 mrad (full angle). The receiver is a 0.5-m diameter telescope with a 0.6-mrad (full angle) field of view. A narrowband filter (0.15 nm) and two crossed polarization detection channels are used. The acquisition system (LeCroy) is based on two 8-bit, 32-MHz waveform recorders.

To reduce the global amount of processed data, the optical, geometrical, and meteorological information has been retrieved from lidar profiles averaged over a 30-min standard period. All clear sky profiles have been rejected. A total of 2770 archived data was obtained. Each archived data is represented by a point in a hyperspace whose coordinates are 80 quantities of possible interest computed for each cloud data.

Cloud base, cloud top, midcloud, and the depolarization peak heights are deduced directly from lidar profiles. For all such levels and for each cloud point the temperature,

Paper number 93JD01476.
0148-0227/93/93JD-01476$05.00